Tutor/s

Dr. Sergi Dosta Parras
Departament Ciència de materials i Química Física

Dra. Camila Barreneche Guerisolí
Ciència de materials I Enginyeria Metal·lúrgica

Grau en Enginyeria Química

Treball Final de Grau

Corrosion resistant thermal spray coatings for protection of TES tanks

Biel Martí Ferré

June 2021

UNIVERSITAT DE BARCELONA

Aquesta obra està subjecta a la llicència de:
Reconeixement–NoComercial-SenseObraDerivada

http://creativecommons.org/licenses/by-nc-nd/3.0/es/

Primerament, m'agradaria proporcionar tot el meu agraïment als meus tutors, que han estat els que m'han ofert la possibilitat de formar part d'aquest projecte, una mica diferent al camp que he estudiat, però que des d'un principi van saber-ho enfocar adequadament.

Per altra banda, però no menys important, agraeixo tot el suport incondicional brindat per la família, amics i/o coneguts els quals han tingut un tracte proper i han mostrat interès i preocupació pels meus estudis.

De la mateixa manera, agraeixo també el suport i implicació que han tingut el conjunt de membres del CPT, per estar a disposició quan ho he necessitat.

CONTENTS

SUMMARY

TES tanks suffer hight corrosion due to the molten salts used in the process. Thermal spray Coatings, especially Inconel 625 superalloys, can be used for protection against corrosion.

In this work, Inconel 625 coatings will be deposited by different thermal spray techniques, including HVOF and CGS.

Then, their corrosion resistance against solar salts and nanofluids will be studied, evaluating if they can be applied as a protective material in TES tanks.

Keywords: Thermal spray, Corrosion, Thermal Storage, Solar energy, Nikel-based Alloys, Coatings, Molten salts, Nanofluids

RESUM

Els tancs d'emmagatzematge d'energia solar tèrmica, estan sotmesos a grans atacats per corrosió degut a les solucions de sals foses en el seu interior. Els recobriments fets amb Inconel 625 poden utilitzar-se per alleugerir els efectes i protegir enfront a la corrosió.

En aquest projecte, es treballarà amb diferents tècniques de projecció, entre les quals es troben l'HVOF o la projecció freda per tal de recobrir substrats d'acer inoxidable utilitzant aquest aliatge en base níquel. Una vegada aplicats, es caracteritzaran i s'analitzarà la resistència a la corrosió en un bany amb nano fluids.

Finalment, els resultats obtinguts permetran comparar les dues tècniques aplicades, i avaluar-ne la possibilitat d'emprar-les com a materials de protecció en els tancs TES.

Paraules clau: Projecció tèrmica, Energia Solar, Sals foses, Nano fluids, Emmagatzematge d'energia tèrmica, aliatges en base níquel, Recobriments

1. INTRODUCTION

Since the beginning of this century, there has been a huge increase in energy consumption on a global scale. The energy requirement is responsible for providing life quality to people, and for driving economic, social, and demographic growth. Nevertheless, the presence of climate change has become a fact that needs to be emphasised to seek solutions firstly.

Nowadays, the most consumed sources of energy come from fossil fuels. Natural gas, coal and oil are prime examples. The combustion of these fuels generates gases such as carbon monoxide and carbon dioxide, among others, which can damage the atmosphere and cause environmental pollution. Gases such as water vapour or CO_2, for example, are responsible for preserving the greenhouse effect [1] and therefore maintaining an ideal temperature for the development of life on Earth. However, it should be borne in mind that a higher concentration in the air of these gases released in the burning of fossil fuels causes an absorption excess of the rays coming from the Sun, a fact that is producing a serious climatic change, increasing the average annual temperature of the planet.

This situation is causing a turning point in the way energy is produced. During this last decade, major transformations and advances in technology are enabling the transition towards the use of renewable energies. [1]

[1] Natural phenomenon in which the normally noxious gases present in the atmosphere absorb solar radiation and increase the Earth's temperature.

The following figure shows the consumption of different energy sources on a world scale.

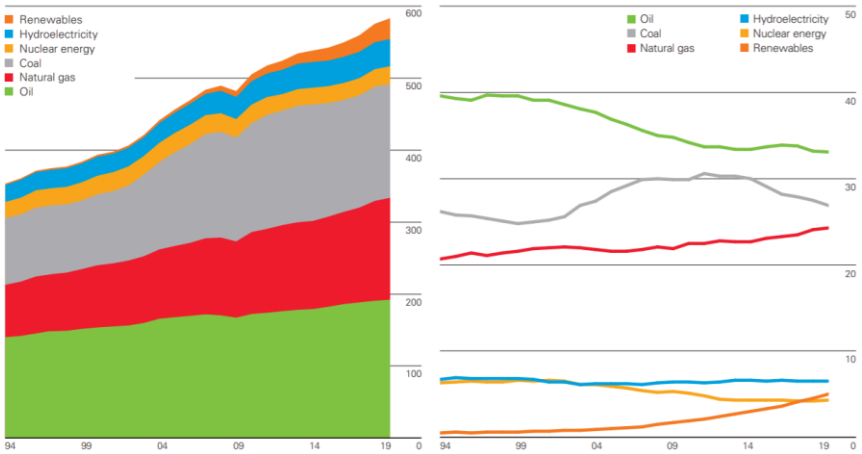

Figure 1. Energy sources consumption on a worldwide scale

(image got from bp Statistical Review of World Energy, 69 Ed, 2020)

The figure is divided into two graphs, the left-hand side shows the change in the evolution of the use of energy sources. The energies that have undergone the most notable change in the last two decades are led by renewable energies, while those that come from fossil fuels maintain a trend similar to prior years.

The diagram on the right shows the percentage share in the total energy mix for each source. The energy consumption of resources such as oil and coal show a clear downward distribution. It can be seen, however, that renewable energies are on an upward trend and their growth is practically exponential[2].

The road to efficiency and a more sustainable world involves the commitment to reduce emissions of nitrogen oxides, sulphur oxides and carbon dioxide, which are emitted in many energy-producing plants. Some of these gases can be very dense and remain in the air, causing phenomena such as acid rain, which is lethal for many ecosystems, both aquatic and terrestrial.[1]

1.1. SOLAR ENERGY, A FEASIBLE ALTERNATIVE

The Sun is a powerful energy-concentrating sphere with a surface temperature of around 5500ºC. Its internal core behaves like a reactor and can transmit a large amount of energy. [3]

The emitted energy shoots out in all directions, a small amount of which is absorbed by the Earth. If it were possible to absorb all the incident energy that is being received in a few minutes, it would be possible to provide all the energy required by the planet in a whole year[4].

To achieve all the environmental objectives that are presented, technology is advancing and the drop in prices on the market means that the possibility of using inexhaustible energy resources as a long-term energy source is no longer just a fiction.

Specifically, in the field of solar energy, the reduction in the cost of solar panels or photovoltaic cells, together with new discoveries in the field of solar energy storage, has helped to open up new production plants around the world, in order to make optimum use of this resource and obtain the highest possible socioeconomic benefit. Currently, there are three different ways in which electricity can be extracted from solar emissions. The most common and most widely used today are concentrated solar power (CSP) and photovoltaic (PV) cells.[2]

PV technology is based on the direct capture of the light emitted by the sun through devices that absorb the photons and convert them into electrons. These cells are usually organised in panels, and are made of silicon or gallium, which are semiconductor materials. This operating method is more applied on a small scale, to fulfil routine needs. The cell technology can be distinguished from CSP by the fact that it uses direct conversion from solar energy to electricity. Photoelectric effect is used for this purpose.

On the other hand, thermoelectric or concentrating solar power plants, also known as CSP (Concentrated Solar Power), operate in the same way as conventional thermal power plants, but their big difference is in the resource they use to generate electricity. Thermal energy uses fossil fuels such as coal, natural gas, or oil, whereas solar power plants use energy from the sun. This technology is typically applied in large-scale plants and high electricity production.

The operation of these plants can be summarised as follows. First, the solar radiation emitted is captured. Then, the rays are concentrated in focal points of smaller surface area to achieve a higher temperature. Then, it is transported as heat using a solar fluid, which will boil water to obtain steam. Finally, this steam acts on a turbine and an alternator to convert it into electrical energy. In this case, solar energy is first transformed into thermal energy and then into electrical one.

There are various types of CSP plants, including parabolic troughs, tower technology, Stirling dish technology and Fresnel concentrators. All of them vary only in the disposition and reception of solar emissions.

As has already been mentioned, during this last decade the great progress in the technological sector has allowed renewable energies to enter the competition for obtaining electricity. However, there are still some challenges to overcome before renewable energies can become a dominant energy source. Like all renewable sources, it is clean and does not emit pollution, but at the same time it is discontinuous. It cannot be used or disposed permanently and is completely linked to atmospheric phenomena, the majority of which depend on the sun. Wind and rain, which are used as renewable resources, originate from climatic conditions caused by the sun[5].

With the aim of taking advantage of solar emissions as much as possible, the concept of energy storage was born. This is when TES (Thermal Energy Storage) technologies came into play.

The solar energy received in the collectors needs to be stored during night hours or other circumstances in which the sun is not present. These systems are capable of keep heat energy in a material for a defined period of time and have the objective of covering the energy needs during off-hours[2].

Solar energy has great possibilities for scaling up and being competitive, but there is still a long way to go and many investments to be made. But in one way or another, this is the progress that will surely have to be done to complete the energy transition that is so necessary for the planet.

---

[2] Timing period in which there is no way of producing electricity.

1.2. **PROJECT CONTEXT**

This study focuses on solar thermal power plants (CSP), specifically on the storage tanks of these installations. TES materials are necessary to achieve greater efficiency and preserve energy reserves as long as possible.

Among the conventional heat transfer fluids on the market, are petroleum-based hydrocarbons, mineral oils or HTFs, and water both in liquid or vapour phase. All of them have some disadvantages that make their application difficult in certain circumstances.

For example, in case of using liquid water, the costs can rise because of the high pressures needed in the process for keeping the water in liquid phase. In the case of steam, the efficiency of the system is low.

A different way for keeping solar energy is to make use of thermal oils. These fluids provide good performance and are widely used as they are non-corrosive, and do not require large pressurisation installations.

When temperatures above 400 degrees are required, it is necessary to operate with other heat transfer fluids. The most promising example, by now, are salts and molten metals. Among the most common used molten salts in industry are those composed of nitrates, chlorides, or carbonates.

These solids are in a solid state at low temperatures and become liquid at high temperatures and low pressures, so they are the best example to choose when working in these conditions.

Another aspect to consider when choosing the best TES material is the compost which forms the tank where these salts will be deposited to maintain energy.

To fulfil the necessary applications, it will be necessary to use materials with good mechanical properties, good corrosion resistance, and good behaviour at high temperatures. Materials such as stainless steel or derivatives can be used in this case.

Depending on the temperature conditions required by the system, one salt or another will be chosen. Usually, nitrate salts are used for temperatures around 450 ºC and chloride salts are used at higher temperatures, around 700 ºC. These salts, when melted, are electrolytes, which are highly reactive, especially with metal substrates.

Recent investigations have been carried out to solve as far as possible these corrosion problems between molten salts and their contact with the tank materials. It has been found that the incorporation of nanoparticles in small proportions into the solutions of the molten salts creates colloidal solutions of nanofluids, where these particles are dispersed[6]. This fact provokes that the oxidative chemical reactions take place in the microscopic levels rather than in the macroscopic ones[7]. That makes improvement of the thermal properties considerably. Additionally, these nanoparticles have a high heat capacity, which is why they are considered to be the best potential solution[8].

Focusing now on the analysis of the project and considering that thermal storage tanks work at temperatures above 400 degrees, it has been simulated the operation of a TES tank working at 450 ºC with a content of sodium nitrate salts and silicon oxide nanoparticles.

2. OBJECTIVES AND WORKING STRUCTURE

The aim of this work is to compare the corrosion resistance of the two spraying techniques applied for the different stainless-steel substrates. The resulting characteristics will be evaluated by means of a molten salt and nanofluids test performed at the same operating conditions of the real TES tanks. Then, it will be determined which one is the most suitable for the working conditions of a thermal energy storage tank.

The content of the work will be divided in two main parts: Firstly, a theoretical one, where thermal spray and its main techniques will be introduced, along with those that have been specifically worked on in this study. The second section will be the laboratory part, where the materials and methods required will be detailed, followed by an explanation of the experimental procedures carried out. Finally, the results obtained will be discussed and the respective conclusions will be made.

3. THERMAL SPRAY

Thermal spray, conceived as a coating technique, has becoming a solid alternative in the world of surface engineering during the last years. Most of industry's fields want to raise their yields and productions to accomplish the globally needs. The efforts to which materials are exposed are ever higher, and thermal spray comes to be a successful alternative to all these demands.

Thermal spray is a technology that uses different types of energy to create a coating line on the surface of the substrates. It is implanted for the protection against high temperatures, to prevent oxidation and corrosion, to improve the properties and to get high quality in a wide variety of materials.

Currently, recent improvements in terms of equipment and materials engineering have enabled thermal spraying processes to find a suitable place in almost all industrial fields, including biomedical, aerospace, power plants, automotive and others. The great diversity of spraying techniques and coating materials that can be machined gives added value to these techniques over others.[9]

Thermal spraying technology has great advantages that make it outstand above many others. Some examples, as well as disadvantages, are described below.

To be able to spray a material properly, it is necessary to work at temperature conditions that are somewhat lower or higher than the melting point of the substance, and it is necessary that the material that is being processed does not decompose when melted. For this reason, a wide range of compounds can be used, such as metals or alloys, or even ceramics and polymeric materials. Among all these, although, the most studied are the metallic coatings.

Another aspect to highlight is the low temperature existing between the interface and the substrate, normally between 100 and 300 ºC. If this temperature were the same than the one at which the projecting pistols operate, which often exceeds 1000 ºC, the microstructure of the substrate could be greatly affected.

Moreover, many of these techniques can be carried out automatically by setting the relevant parameters in advance. This functionality allows to set a thickness to project and the exact area where to do it, make that its applications even more flexible[10].

On the other hand, this technology has a couple of disadvantages including a low process efficiency coefficient and rough working conditions. During a thermal spraying process, the machines used could be very noisy and dusty, and could affect human health[11].

3.1. PRE-SPRAY TREATMENT

Before starting a thermal spray process, it is necessary to complete several preliminary procedures.

The material to be coated may come from different origins, many of them can have already been coated and presents some parts uncovered. Others could have wear in different parts, and it is necessary to re-spray the coating to increase the useful life of the material and protect better the substrate.

On the other hand, it is possible to find samples with grease that needs to be removed. For this reason, in a first stage, the objective surface has to be cleaned with some organic solvent. Following this, a shaping process is applied so as to obtain the appropriate dimensions for processing the samples.

Finally, the pre-processing is finished with the activation of the substrate surface. It is very important to carry out this step just before the projection process, as it is at this point where the necessary roughness is created so that the projected particles can adhere correctly. This last step is carried out by shot blasting with alumina.[9]

3.2. **THERMAL SPRAYING TECHNIQUES**

As mentioned before, in a thermal spraying process, the feedstock is sprayed directly onto the surface of the substrate by capturing energy from various external sources. Essentially, the particles must be plastically deformed in order to adhere into the substrate surface. Various parameters must be controlled for this purpose, where temperature provides the thermal energy and velocity generates the necessary kinetic energy.

Industrially, there is a wide variety of thermal spraying techniques, but they mostly differ in the source of energy used in each case to fire the recovery on the substrate.

Among the most commonly applied techniques today, the following stand out: Flame Spraying (FS), Atmospheric Plasma Spraying (APS), Hight-Velocity Oxygen-Fuel (HVOF), Cold-Gas Spraying (CGS).

Basically, the flame technique, which was one of the first techniques developed, uses the energy emitted in the combustion of gases to generate a flame that melts the particles and accelerates them towards the substrate with a torch.

In contrast, in the case of the APS technique, electrical discharges of ionised gases in a plasma state are used to produce thermal energy.[9]

This study focuses on the latter two techniques, HVOF and CGS, which will be discussed in more detail in the following chapters. [12]

3.2.1. HVOF

HVOF spraying is considered one of the most advanced techniques and has a high potential of application among all thermal spraying techniques. [13]

First developed in the early 1980s, it is considered a relatively recent spraying technique, which improves the properties of its previous technique, the detonation gun or D-Gun Spray.

It belongs to the family of techniques that use the energy produced by the combustion of gases to generate a coating layer over the surface of the substrates.

Unlike the Flame Spray technique, it works at a higher impact speed and the temperatures are lower.

During a HVOF method, fuel and oxygen are introduced into the combustion chamber together with the powdered coating.

The continuous burning causes a large increase in temperature and pressure inside the chamber up to a value of 3000ºC and 40 bars respectively, where the powder particles almost completely melt.

The final operating values are related to different parameters, which makes the optimisation of this process more complex.

In the next figure, HVOF method where powder impacting perpendicularly towards the workpiece is presented.

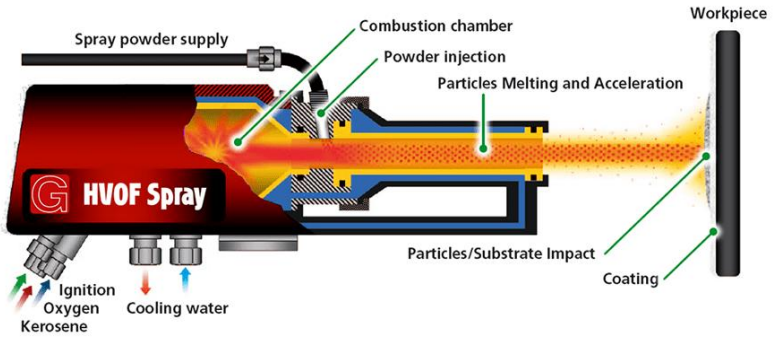

Figure 2. HVOF technique equippment

(Image got from Griekspoor Thermal Coatings[33])

The spraying velocity is up to 1000 m/s, supersonic, and can be controlled by many factors. The pressure gradient between inside the chamber and outside is an obvious example, because if high pressures are achieved, the particles will have a higher exit velocity. An important operating parameter is the nozzle3 geometry, which can have a convergent or divergent profile.

There are much more variables that affect the quality of the deposited coating. The size of the feedstock, the direction and angle of spraying, the distance between the spray samples and the gun, etc.[14,15]

The properties of the coatings produced by High-Velocity Oxygen Fuel have high density, presenting porosities below 2% on average, hardness, and a good resistance to high mechanical stresses.[16]

When working with the HVOF technique, it is also important to keep in mind that the thermal energy is provided by the combustion of oxygen. The powdered feedstock gets in contact with the mixture at high temperature which can produce oxidation in some areas of the samples.

3.2.2. CGS

The Cold Gas Spray technique, also known as cold projection, was firstly discovered in th 1980's, but it was not until the 90's when was summited into several investigation due to the promising features that seemed to have. [17]

Nowadays, it can be considered as a new alternative of the HVOF Spray, but essentially differs mainly in the production of the energy needed to carry out the process. This technique uses the kinetic energy that has been generated through the heating of inert gases to accelerate the particles.

Typically, the gases used in these processes are nitrogen and helium. During the operation process, these gases are introduced into a heater that increases the temperature and drives them into a cylindrical nozzle, with a convergent-divergent profile. This geometry is key to accelerate the resulting mixture. [18]

---

[3] Final cylindrical part at the end of a torch or gun that controls the ejection of liquid or gas.

In the contact point between the powder and the gas, the shape is convergent, and the velocities are close to the sonic speed. After that, it expands rapidly to increase the velocities even more.

The temperatures reached are lower than the melting values of the primary material. As mentioned above, on one hand, inert gases are used, which do not react with the recovery. In the other hand, no particles are melted, which means that there is no phase change. The particles adhere to the substrate surface by plastic deformation. For this reason, in many cases where CGS is used, it is not necessary an alumina blasting to provide roughness.

This technique has been extensively studied, and it has been proven that it can be applied on both metal and ceramic substrates.[19]

As in HVOF Spray, the chemical composition of the gases, the used material, the pressure and temperature, the type of nozzle or the material that acts as a coating are many of the changeable factors that can affect the quality of the coating.

Finally, the recoveries resulting from CGS have low porosities, high density and very low oxidation.[20]

4. EXPERIMENTAL SECTION

On this section the experimental process of the study will be discussed, as well as the materials and methods used to obtain the respective results.

The experimental processes and operations that will be mentioned were mostly developed at the facilities of the CPT (Centre de Projecció Tèrmica) of the University of Barcelona, and some of them were carried out at the BioPol Center, an adjunct laboratory of the CPT located at the Bellvitge campus.

4.1. **MATERIALS AND METHODS**

For the experimental part of this work, it was necessary to use a combination of materials consisting by stainless steel metallic samples and an Inconel 625 alloy, acting as a coating. Different considerations had to be taken to select these materials rather than others. The study has been performed under conditions previously mentioned, more than 400 ºC and in a nanofluid bath. The material needed to have good physical, mechanical and chemical characteristics, which finally selected steel as the best material.

Following the aim of the work, it has been decided to select a coating made from Inconel 625 powder (Diamalloy 1005 from Sulzer Metco (Pfäffikon, Freienbach, Switzerland), a nickel-based superalloy, normally symbolised by NiCrMo. Many studies have proved the good performance offered by this material[21]. Its high composition of nickel and chromium offers high resistance in oxidising environments, and the combination of nickel and molybdenum provides huge resistance to mechanical stress and high temperatures[21].

According to the work's purpose, stainless steel, specifically AISI316, was selected as a substrate material, mainly because of his real application in the chemistry and materials engineering field. As a matter of fact, Stainless steel has been the most selected material for the construction of TES tanks and other plant's equipment. This material has good chemical and mechanical properties, including the ability to withstand high temperatures, and its resistance to chemical acids and corrosion.

Stainless steel is obtained from an alloy consisting mainly of iron, chromium, and nickel, and has a low carbon composition, around 0.1-0.2%. The nickel gives good resistance to high temperatures, and the chromium reacts with the oxygen in the air to form a layer of chromium oxide, which passivates the steel and protects the surface.

For the execution of this work, different samples of stainless steel were initially subjected to a shot blasting process and then coated using two different spraying techniques, HVOF and CGS.

For the corrosion tests of the samples, the specimens have been subjected to a molten salts bath. Three replicates, each providing results at different times, would have to be done to check the accuracy of the results. Due to time limitations, it was possible to obtain the results of one replicate and put a second one on process, which cannot be commented in this study. At the end of the second replicate, a final retest will be carried out to confirm the results.

Out of work's scope, a carbon steel F111 substrate, which is used for very general purposes, was also included in the corrosion test. The non-ideal properties of this carbon steel make that the possible obtained results with this material would not be applied for this project, as the main goal is focusing on the stainless steel, which is the one used in the TES tanks.

For the structural characterization, different methods have been applied in the different stages of the experimental work, including optical microscopy (OM), SEM and FE-SEM electron microscopy for the microstructure analysis.

X-ray diffraction analysis (XRD) will also be evaluated for characterizing the crystalline phases of the samples. DRX process consists in a stream of light projected onto a sample to be analysed. Depending on the intensity received and the incidence angle, a signal is produced which, on passing through a detector, creates a peak in the chromatogram. These graphs show the relative intensity in relation with the incidence angle of the sample.

Furthermore, a Laser Scattering (LS) for the Inconel 625 raw material has been applied to get an initially recognizable value of the particle size.

In the following sections, each method used on the procedure will be explained in detail.

4.2. EXPERIMENTAL PROCEDURE

4.2.1. Surface activation

The first step in the experimental process was the preparation of the samples before projection. For the stainless-steel samples which were desired for HVOF process, with dimensions of 5x5x0.5 cm, the cutting process was applied to reduce their amplitude to 3 cm, ending up measuring 5x3x0.5 cm. In the prove with carbon steel, the size of the pieces was 5x2x0.5 cm. In the other cases, the dimensions did not change since the initially dimensions of approximately 5x2x0.5 cm.

A set of approximately 15 specimens of stainless steel and 5 of carbon steel were shot-blasted with alumina (Al_2O_3) using the MAB-4 equipment (CPT, Barcelona), to activate the surface, promote surface roughness, and remove the oxidation. An indentation test was conducted with a Vickers test stick to ensure the adhesion of the recovery.

Furthermore, a pair of Inconel625 bulk pieces were necessary to prepare and be compared with the Inconel 625 coating deposited over metal substrates. For this case, it was not necessary to apply any alumina-blasting process.

4.2.2. Initial powder analysis

The coating layer has been made of Inconel 625 in powder form, obtained through an atomisation process. Its 1350ºC melting temperature provides excellent resistance to high temperatures, oxidation, and corrosion.

The nominal composition of this compound is listed in Table 1.

Table 1. Weight composition of Inconel625 powder

Compound	Nickel	Chromium	Molybdenum	Niobium/Thallium	Iron
wt. [%]	63	21,5	9,0	4,0	2,5

The Laser Scattering (LS) technique was used to calculate the particle size distributions by means of the Beckman Coulter LS Particle Size Analyzer, which provides the average diameters and the respective percentages. [22]

For the characterisation of the sample's free surface, an enough quantity of powder was placed inside the mounting equipment. Conductive resin was added, and it was treated with grinding and polishing processes before being subjected to SEM microscopy.

Finally, X-ray diffraction (XRD) techniques were applied to observe the crystalline phases in which Inconel625 powder is composed.

4.2.3. Spraying operation procedure

Nickel-based superalloy powder was selected as the raw material for thermal spraying onto stainless steel substrates using HVOF and CGS techniques.

The Inconel 625 powder applied by HVOF was sprayed using the Plasmatechnik CDS-100 equipment, employing propylene as a fuel gas, oxygen as an oxidant, and nitrogen as inert gas.

Figure 3. HVOF spraying chamber (CPT Barcelona)

The spraying processes are executed in a pressurised chamber, where the refractory materials are fired with spray guns towards the samples. Due to the high operating temperatures, it is necessary that the background, where any flame or spray may end up, is refractory or metal with high melting temperatures.

In the case of the CGS, the particles were sprayed with KINETICS 4000 (CGT, GERMANY) Cold Gas Spray equipment included the D24 WC nozzle. The used parameters are summarised in table 2.

Table 2. Report of the CGS operating parameters

Variables	Value
Working Pressure [bar]	64
Process gas	N_2
Feeding rate [mm/s]	500
Operating temperature [ºC]	1000
Spraying distance [mm]	20
Efficiency [%]	53
Nozzle	Long Glass

In the case of CGS, it is important to underline that the first samples were produced at 55 bars of pressure. A study of the efficiency between this value and the one shown in the table 2, was made, and it was found that the optimum results were to work at higher pressures. This can be explained by the fact that the gas pressure was higher, and the velocity increased, promoting better deformation of the particles after impact on the substrate.

4.2.4. Samples characterization before corrosion test

Once the spraying process was finished, the specimens were analysed before being subjected to the corrosion test.

The characterisation of the samples was performed according to the sequence defined by the ASTM standards, which establishes the correct metallographic preparation for analysing the coatings[23].

The first step was to obtain the cross-section. The equipment used was the cutting machine ABRASIMENT 250 (CPT facilities). In this process it is important to consider different aspects to avoid excessive wear of the piece. Depending on the necessity required or the material applied, the abrasive disc can be selected, as shown in table 3.

Table 3. Selection of abrasion disc related with the material used

Type	Reference Number	Materials
07P	102507P	Ductile materials
HHA	60A25 (STRUERS)	Superalloys such as Inconel
HH	40A25 (STRUERS)	Hard ferrous materials
H	95-B2203	Soft ferrous materials
NF	95-B2205	Non-ferrous materials as Cu

In this case, the abrasive disc 60A25 (Cut-off Wheel, Struers, CPT facilities) was used, designed for very hard metals and alloys such as Inconel.

Afterwards, the cross sections (ST) were mounted on the LaboPress-3 equipment (Struers, CPT) with fine conductive cold resin.

The operating parameters were 180ºC, a heating time of 4 minutes, a cooling time of 2.5 minutes and a load of 20 KN.

The process continued with a grinding with abrasive silicon carbide papers (CarbiMet, BUEHLER) following the sequence 120,240,360,600,2500, where the higher number represents major purity and the lower, more roughness. Various investigations have allowed us to conclude that it is better to use the automatic roughing machine, as it reduces inconsistencies and avoids irregularities in the thicknesses of the recovery (see ref.).

The last step before the OM process, was to polish the samples with 6 µm and 1 µm diamond suspensions (MetaDi, BUEHLER). Both grinding and polish processes had an approximately duration of 8 minutes for each step.

For the coating characterisation, two samples of each spray technique were used, one for optical microscopy and one for electron microscopy and XRD.

The Leica DMI5000M inverted optical microscope was used for the metallographic analysis, evaluating the thickness and consistency of the recovery.

The free surface was characterised with the Phenom ProX Desktop SEM (Scanning Electron Microscopy), which allows in-depth results to be obtained.

Finally, with the XRD equipment PANalytical X'Pert PRO MPD (PANalytical), the different crystalline phases of the recoveries were provided.

4.2.5. Corrosion test

According to the objective of the study, a corrosion test was developed taking these considerations into account.

To establish comparisons, the test was carried out on stainless steel and Inconel bulk substrates. Thus, it was possible to compare the efficiency of the coating incorporation, improving successfully or not the final properties of the material.

In addition, the HVOF and CGS spray on steel substrates have been applied to one side, so that it has been necessary to protect the opposite part with an appropriate material.

For this reason, prior to the immersion of the samples in the molten salts bath, it was decided to use an adhesive paste resistant at high temperatures (Nural 30, PATTEX). This product must be kept in a cold atmosphere, to prevent solidification. This thermal paste were applied to all the reverse sides and to all the substrate's corners that were not coated, to avoid excessive damage of the steel.

The corrosive test was performed by means of a nano fluid bath. Therefore, 4 crucibles were prepared with the liquid solutions inside. The temperature of the oven was set at 450 ºC, and two separate studies were conducted with different exposition times. For each test, an enough quantity of nanofluids was introduced to cover 2/3 of each sample when placed inside crucible. Thus, one part would be in contact with the corrosive salts while the other would not.

In the first test, the materials were kept immersed in the water for a period of one week, but the second was done in a period of one month.

According to the materials used for the assay, it was necessary to use sodium nitrate (from Sigma Aldrich, 99.995% pure) and silicon oxide nanoparticles with a variable diameter between 5 and 15 mm. A 1% proportion in weight of nanoparticles was considered in the final solution that was later put into the oven.

The preparation process of the nanofluids can be described in the following way. First, a quantity of 76 grams of sample was prepared, and then solved in about 30 ml of water. Continuously, an interval of time was given to allow the nanoparticles diffusion and homogenize the solution. Finally, the solution was summitted to a temperature of 100ºC, evaporating the solvent and recrystallizing the solution.

4.2.6. Characterization after corrosion test

The characterisation of the samples after corrosion tests consisted in a similar procedure to the analyses prior to the corrosion assay. The same methods were applied to the one-week and one-month samples.

After letting cool the samples, two slices were taken for the part that had been in contact with salts and two more for the one which was not.

One of the pieces of each part was prepared for microscopic observation (mounting, grinding and polishing) on a transversal surface, in order to see the thickness loss generated by the nitrate bath.

The other cut of the two parts was used for the observation of the free surface with the SEM and FESEM microscopes, and then sent to XRD. To get available results, the sample observed must be conductive, as the SEM and FESEM work with electron scanning. After the immersion of the samples in the bath, oxides could form there, which constitute non-conducting ceramic materials. Therefore, to observe these samples under the microscope, a sputtering process had to be undertaken with a thin gold layer and graphite evaporation.

5. RESULTS AND DISCUSSION

In this section, the results that have been found in the experimental part will be presented and commented based on the concepts analysed in this study. It has been decided to follow the same structure used in the previous section to better classify and structure the results.

It is especially important to point out that in this section, the characterisation of the free surfaces will be based on comparisons between samples that have been in the oven for a week, showing the difference between the parts in contact compared to those that have not. For the cross-sectional surfaces, it will be reflected the results obtained in each test.

In the case of the XRD diffractograms, the samples will be compared in the one-month corrosion study, considering that if there has been a phase change, this will be more visible after one month.

5.1. **POWDER CARACTERITZATION**

The Beckman Coulter analyser (CPT facilities) provided the information about the Laser Scattering applied to the atomized particles of Inconel 625 powder. The resulting distribution is shown right below.

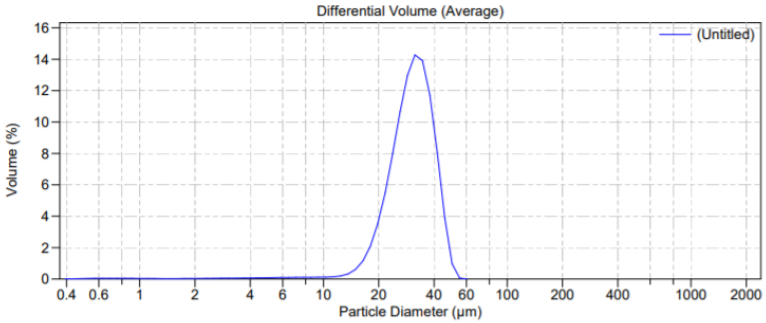

Volume Statistics (Arithmetic)

Calculations from 0.375 µm to 2000 µm

Volume:	100%		
Mean:	30.55 µm	S.D.:	8.305 µm
Median:	30.66 µm	C.V.:	27.2%
D(4,3):	30.55 µm	Skewness:	-0.383 Left skewed
Mode:	31.50 µm	Kurtosis:	0.785 Leptokurtic

d_{10}: 20.72 µm d_{50}: 30.66 µm d_{90}: 41.22 µm

Figure 4. Laser Scattering of the Inconel 625 powder

The observed trend has a Gaussian shape, which is explained by the random dimensions in the selection of the particles to be analysed. D_{10}, D_{50} and D_{90} are parameters that indicate the particle diameter of a 10, 50 and 90% of samples' volume is evaluated.

In addition, another significant result exported from this analytical dispersion was the median value, which was 30.66 µm.

Free surface of Inconel powder samples was characterised using SEM microscopy.

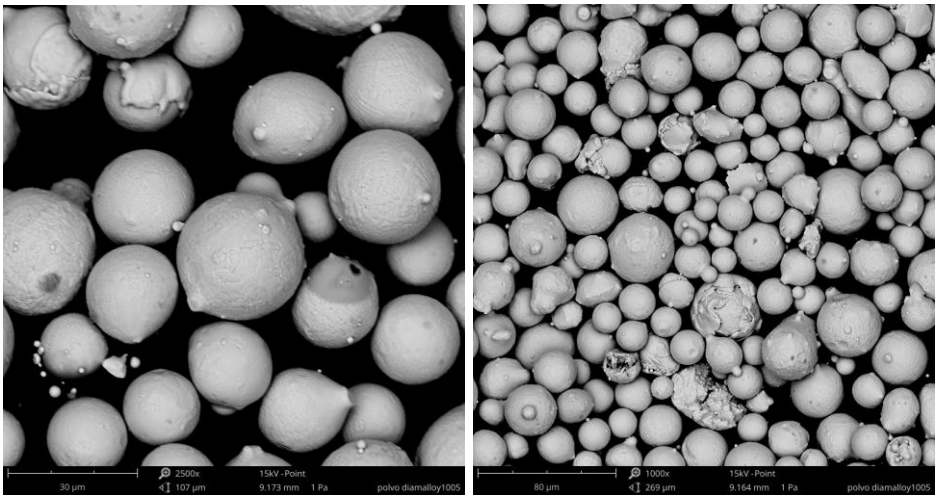

a) *b)*

Figure 5. SEM free surfaces of an Inconel625 taken at ***a)*** 2500 magnifications, ***b)*** 1000 magnifications.

The images with depth and taken at different magnifications, showed the spherical morphological character of the particles. According to the Laser Scattering results, it can be confirmed that the particle size is considerably different from each other.

The crystalline phase analysis of Inconel powder will be discussed later by comparing it with the bulk Inconel sample, which was immersed in the nanofluid bath for one month.

5.2. **COATINGS CARACTERITZATION BEFORE CORROSION TEST**

In this section, the microstructural analysis realised over the initial sprayed samples is commented.

The characterisation of the Inconel 625 overlay using HVOF and CGS onto the stainless-steel substrate was studied.

Optical microscopy observations enabled to measure the thickness of coatings and characterise the interfaces between the substrate and the Inconel625 (Figure 6).

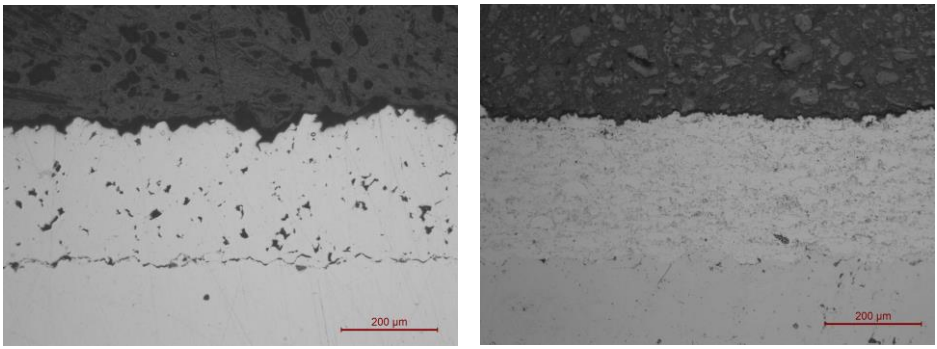

a) *b)*

Figure 6. Cross-section of *a)* CGS Inconel625 coating, *b)* HVOF coating

The coatings made with both techniques show satisfactory adhesion to the substrate surface, a fact that can be explained by the surface activation with alumina.

Comparing both techniques, it can be observed that the interface between stainless steel and Inconel is clearer in the case of HVOF, compared to the CGS, where it is sharper.

In the case of high velocity-oxygen fuel, the fusion of the particles has caused better adhesion, but at the same time, more oxidised zones have been formed.

In the case of cold spraying, the recovery seems to be more porous than in the HVOF technique. To check that, it has been decided to use the IMAGE J software to estimate the porosity in both cases (Figure 7, table 4). Three different measurements have been taken in a different coating area for each coating technique applied.

As an example, the sequence of images captured by the Image J software in the porosity estimation of the CGS sample is shown in figure 7.

The portion of the sample to be analysed is selected, and the range of pore coverage can be selected manually. Then, based on the area differences, the software calculates the porosity percentage of the sample.

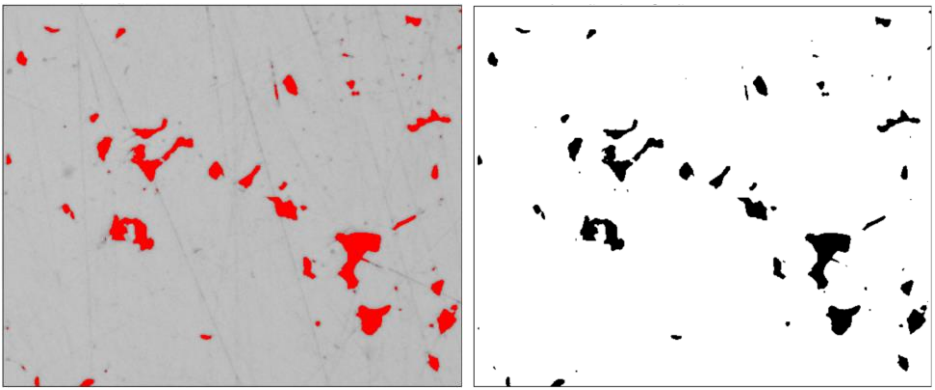

Figure 7. Sequence of porosity measurement of CGS sample

It should be remembered that in the CGS technique, the recovery particles are deposited by deformation, not by melting. Therefore, it is highly possible that some solid Inconel particles may have been removed during grinding process, since many porous zones have similar dimensions to the initial calculated powder and have spherical shapes.

This is an important fact, because the way in which porosity was measured in CGS coating did not contemplate the effects of ripped particles. Therefore, the real results are lower than those reported in the next table.

Table 4. Porosity results

Porosity [%]	**HVOF INOX**	**CGS INOX**
Medium value [%]	0,64	4,30
Standard deviation [%]	0,32	0,42

A total of 40 different measurements were taken with the software to obtain a representative value (see annex 2) of the mean coating thickness and the standard deviation, which are tabulated below.

Table 5. Thickness reports

Spray technique	HVOF INOX	CGS INOX
Coating thickness [μm]	288.352 ± 12.942	264.370 ± 20.142
Standard deviation [μm]	12.942	20.142

The differences between the coating's thicknesses may be due to the different spraying conditions, since in each case the recovery is adhered through different ways.

In relation to the standard deviations, it can be noticed that the recovery made with CGS presents more irregularities and presents more variation than the one made with HVOF, which is denser and consistent.

The free surface observation of the two As Sprayed[4] samples through SEM microscopy allowed to take photographs with high depth of focus and study the microscopic structure.

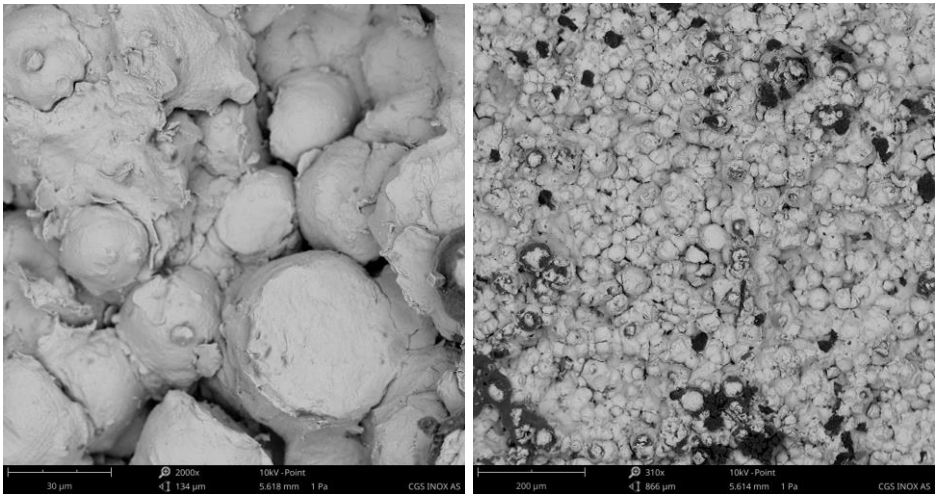

8 a) *8 b)*

Figure 8. SEM free surfaces of a CGS Inconel sprayed over stainless-steel substrate at *a)* 2000 magnifications, *b)* 310 magnifications.

[4] Inox substrates coated by Inconel and not submitted to corrosion test

In this first case, the disposition of the particles sprayed by CGS showed that the spherical shape of the initially designed particles remained constant. Observing at low magnifications, the porosity of this coating is reflected, as discussed before. Going at upper magnifications, it is possible to see that the inter-particle zones are a bit uncovered.

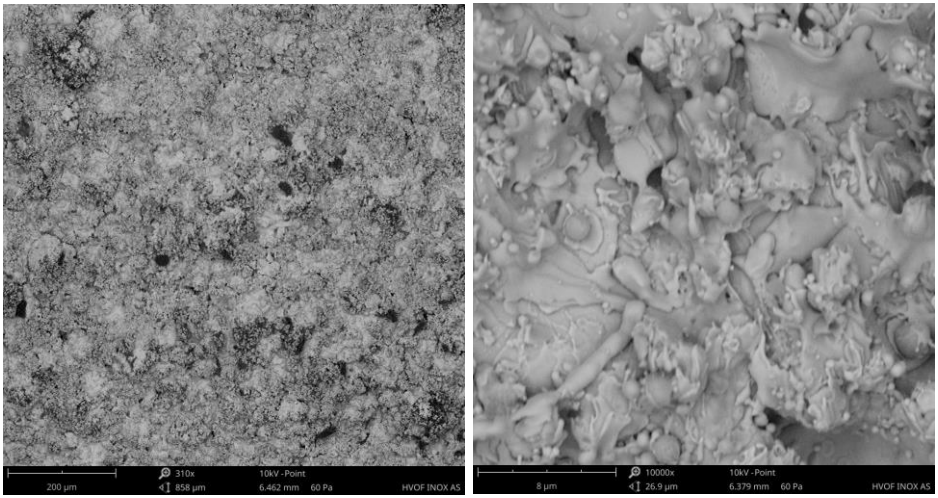

9 a) *9 b)*

Figure 9. Samples free surfaces made by HVOF Spray.

In the HVOF coatings, the fusion of the particles before impact generates the formation of splats with an elongated character. The images shown in figure 9 demonstrate that the superposition of the splats has created a consistent distribution of the coating without uncovered interparticle spaces.

In respect with the crystalline phases, they were analysed using X-ray diffractometry, and the results will be comented through the comparison with one month corrosion test samples.

5.3. FINAL CHARACTERISATION AFTER CORROSION TEST

After the corrosion tests, the samples were characterised to determine if they were resistant or not in the nanofluid bath. For the comparisons made in this section, it was considered that the As Sprayed samples were those that were not submerged in the salt (non-salt parts).

That consideration has been checked later because of the incoherent results obtained before, which used the AS-SPRAYED samples (those before corrosion tests) as initial ones.

The samples were analysed through optical microscopy to calculate the thickness reductions in the coatings and characterized the coating behaviour.

The first evaluation will be done over one week corrosion test and then, finalizing with the one-month assay.

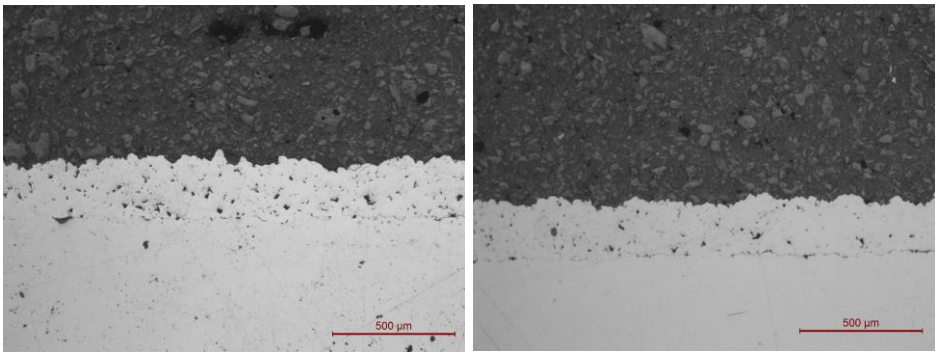

10 a) *10 b)*

Figure 10. Cross-sections of the CGS INOX 1 week test *a)* sal part, *b)* non-salt part

For the one-week samples, sprayed with CGS, no major differences were observed between the two parts. The part that was in contact with the molten salts seems to have experienced a little increase in porosity, probably due to the particle removal caused by the corrosive environment.

The average thicknesses and the standard deviation were calculated by making 30 measurements of each part, and it was possible to verify that there were almost no differences between both samples.

Table 6. Thickness mesurements of Cold Spray coatings

Sample	CGS INOX SALT	CGS INOX NON-SALT
Coating thickness [µm]	222.160 ± 21.294	223.368 ± 25.903
Standard deviation [µm]	21.294	25.903

With the HVOF coatings, the following cross-sectional results were reported.

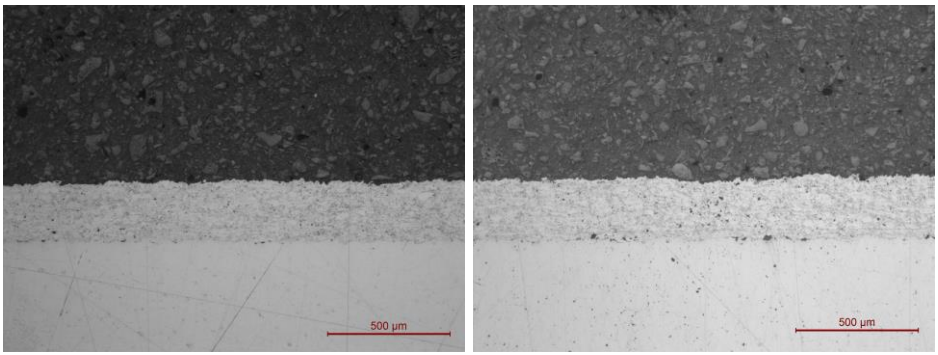

11 a) *11 b)*

Figure 11. Cross-sections of HVOF 1 week samples a) non-salt side, b) salt side

The high-velocity coating spraying provides very dense results with little porosity. After a week's treatment, the thickness remains stable, as shown in table 7.

Table 7. Inconel 625 HVOF INOX thickness coating reported on one-week corrosion test.

Sample	HVOF INOX SALT	HVOF INOX NON-SALT
Coating thickness [µm]	246.086 ± 8.777	247.253 ± 12.014
Standard deviation [µm]	8.777	12.014

After the one-month corrosion test, the thickness reductions were recalculated, also using 30 optical measurements, and the structures were characterised.

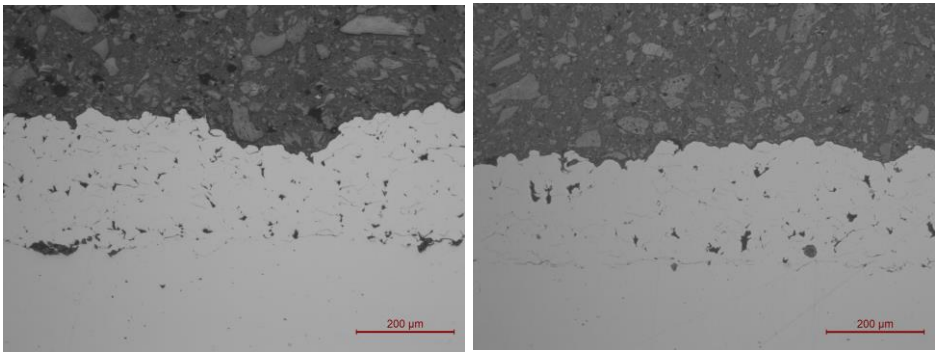

12 a) *12 b)*

Figure 12. Cross-sectional of the CGS a) salt side, b) non-salt part

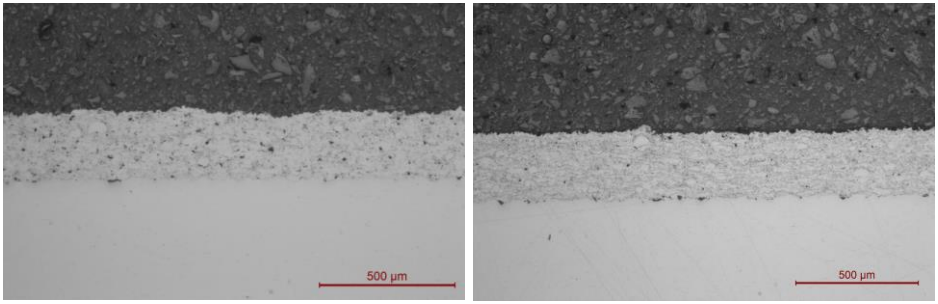

13 a) *13 b)*

Figure 13. Both HVOF coating a) salt side b) non-salt side

In the representation of the coating sprayed by CGS, in the salt part, a large reduction in thickness can be reflexed in some points more than in others. In the interface Inconel-stainless steel, the formation of more holes where previously some particles were located have been promoted by the corrosion bath.

In the HVOF coatings, it can't be seen a notable change on thickness, and the interface is still well connected to the substrate.

Subsequently, the thickness reductions results over the stainless steel substrate, have been tabulated together, for both tests and techniques applied.

Table 8. Inconel thickness report

Coating Thickness reduction [µm]	**1 week corrosion test**	**1 month corrosion test**
HVOF INOX [µm]	1.168	14.051
CGS INOX [µm]	1.208	9.275

On the other hand, for establishing the thickness reduction on the Inconel bulk (Inc B) sample, it was necessary to use an automatic vernier caliper, because of the little dimensions provided by the optical microscope to cover the entire 5 mm thickness of the piece. The obtaining values from both corrosion tests (1 W and 1 M) are tabulated below.

Table 9. Reduction thickness of Inconel Bulk on the different corrosion tests

Measure	Inc Bulk 1 W salt	Inc B 1 W Non-salt	Inc B 1 M salt	Inc B 1 M non-salt
Medium [mm]	4.82 ± 0.01	4.90 ± 0,01	4.84 ± 0.01	4.91 ± 0.02
Reduction [mm]	0.07		0.07	
Reduction [µm]	74		74	

According to the results achieved from the thickness reductions, it is found that by using Inconel Bulk without substrate, the thickness decreases are almost an order of magnitude higher.

In accordance with the aim of the work, and in line with an economic philosophy, it has been demonstrated that the use of Inconel as a stainless steel coating provides better corrosion resistance than if the superalloy was used alone.This fact is justified by the manufacturing process of the inconel or the substrate[24]. Moreover, the use of Inconel bulk as a protective material would entail a much higher construction cost.

Finally, literature research has been undertaken in order to find the corrosion of stainless steels[25]. It is important to always be aware of the operation conditions, which in this study, has been the accelerated corrosion with molten salts bath with nanoparticles, and at 450 ºC. The values found in different investigations have allowed to consider that a stainless steel under these conditions has a corrosion rate that can reach 2 mm/year[26–28]. If it is taken into account that the implementation of Inconel 625 protects the substrate and provides an approximate corrosion value of 10 microns/month, every year it could lose 100 microns, considering a linear thickness reduction[29,30]. This leads to deduce that the application of Inconel as a coating material is so interesting.[31,32]

For microstructural examination and characterization, photographs were taken with FESEM electron microscopes to analyze the free surfaces of the samples from the one-week corrosion test and compared them with the non-salt pieces. SEM microscopy was applied for the cross-sectional observation. It was not possible to analyze the free surfaces of the one-month samples because there was still no scheduled day to go to FESEM.

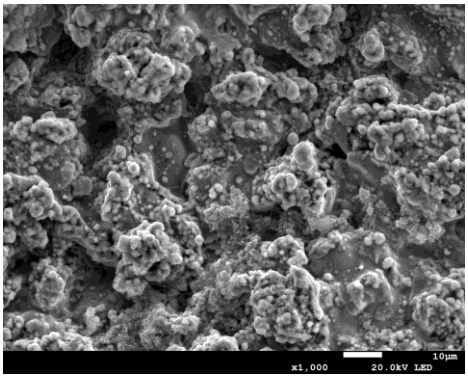

14 a)

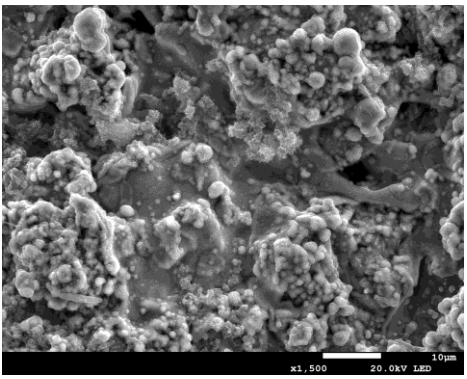

14 b)

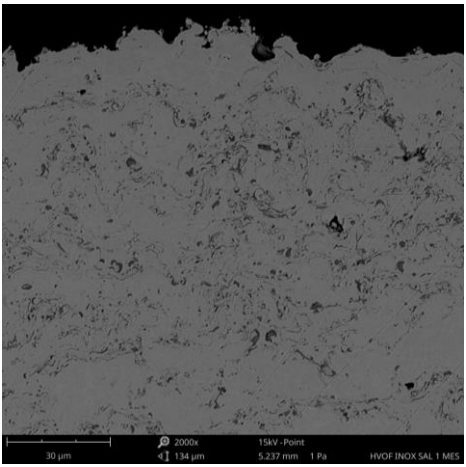

14 c)

Figure 14. a) and b) show HVOF INOX one week corrosion test free surfaces taken by FESEM at different magnifications. c) HVOF one month corrosion on cross-sectional vision with SEM

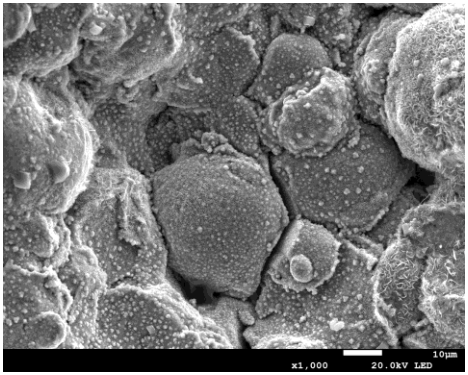

15 a)

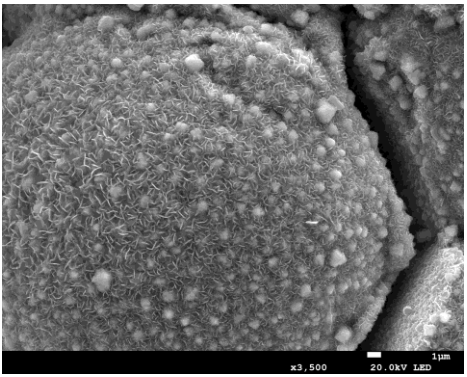

15 b)

The good quality and precision of the images taken by FESEM enable to observe the formation of surface oxides. in the case of HVOF, it can be observed the irregular shapes of the splats generated when spraying and if it is compared with the images of figure 9 b, the corrosion is present on the surface in the form of white colors. In the case of the spherical particles of c, the presence of oxide surrounding the particles in the form of pitting can be greatly appreciated.

Through the observation of the transversal surface, it can be seen that in the case of HVOF, there has been no penetration of the corrosive medium through the coating layers close to the substrate. On the other hand, in the CGS, the nitrate salts are penetrating through the spaces between particles until they practically reach the stainless steel. this could lead to long-term decohesion.

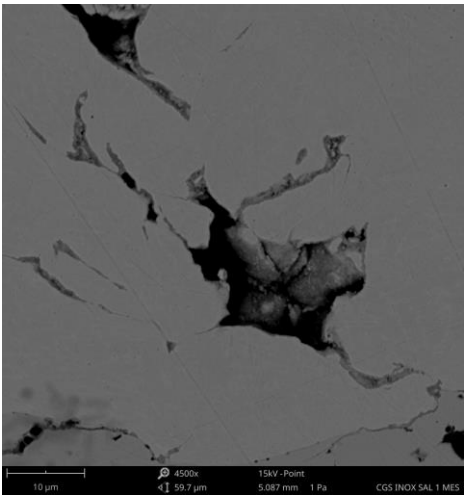

15 c)

Figure 15. a), b) reflex CGS INOX 1 week corrosion in a FESEM microscopy. c) shows a cross-sectional aspect taken with EM after one month corrosion test

Finally, the crystalline phases have been analysed using X-ray diffraction. Typically, a copper line is projected on the surface of the sample and the diffractions of the light are observed. The X'Pert software has an incorporated database in which, depending on the relative intensity and the diffraction angle, it analyses absorption peaks.

The following results have been obtained by comparing the As Sprayed specimens with the corrosion ones during one-month tests.

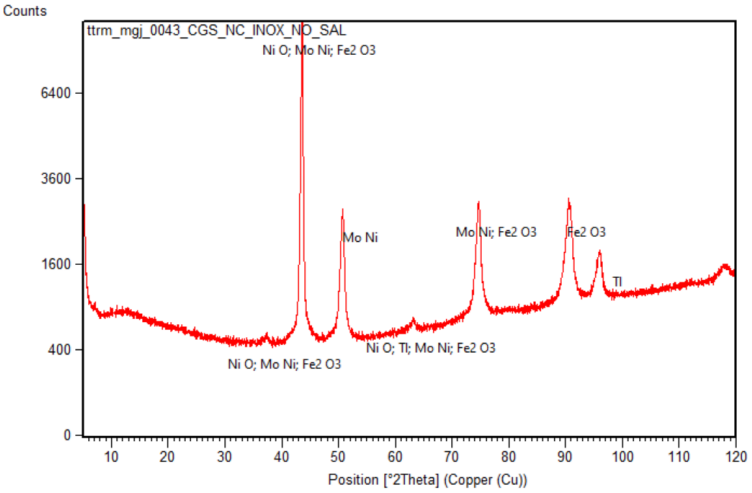

16 a)

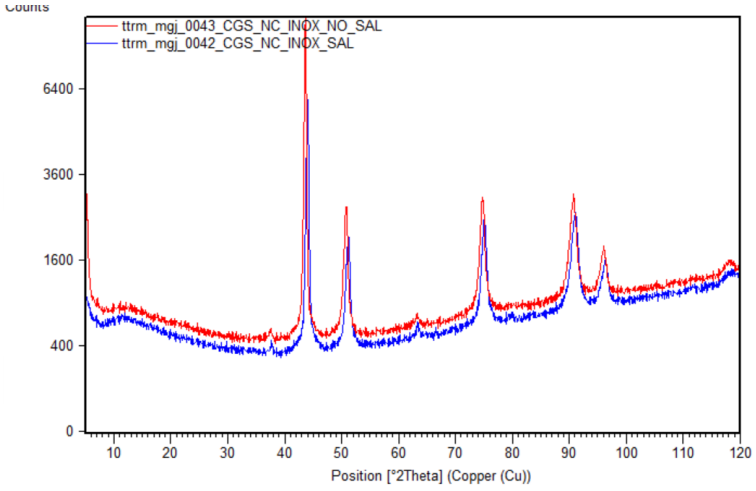

16 b)

In the first two diffractograms, it can be seen that the absorption peaks formed in the cgs samples of the part immersed in salt and the part that has not, do not present any substantial changes.There are 5 main peaks, with majority phases of iron and nickel oxides, because even though they have not been in contact with the salt, nitrate vapours have been generated at high temperatures, thus oxidising pure crystalline phases of inconel. Also, pure phases of nickel, molybdenum, thallium, the main bases of inconel 625, can be seen.

Tthe comparison shows that the phases have not changed, a fact that can be justified by the good surface corrosion resistance of CG Spray.

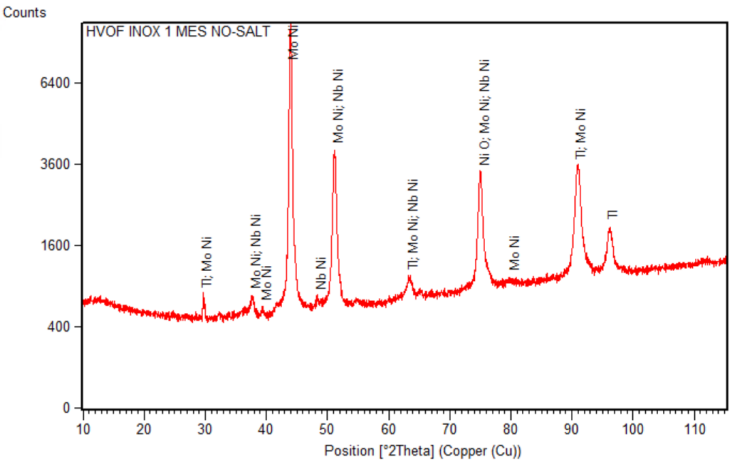

17 a)

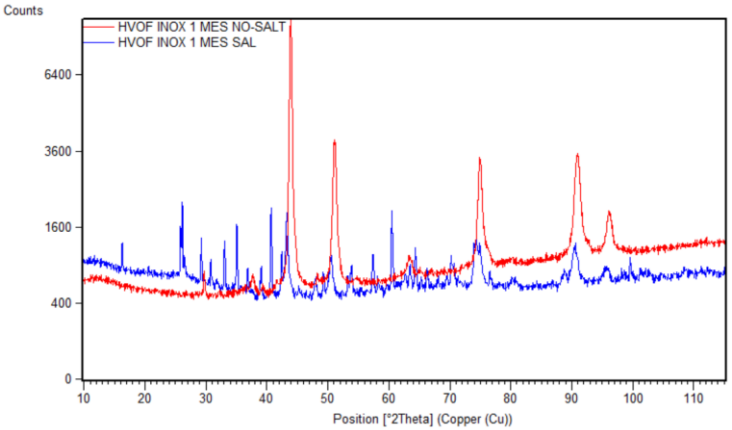

17 b)

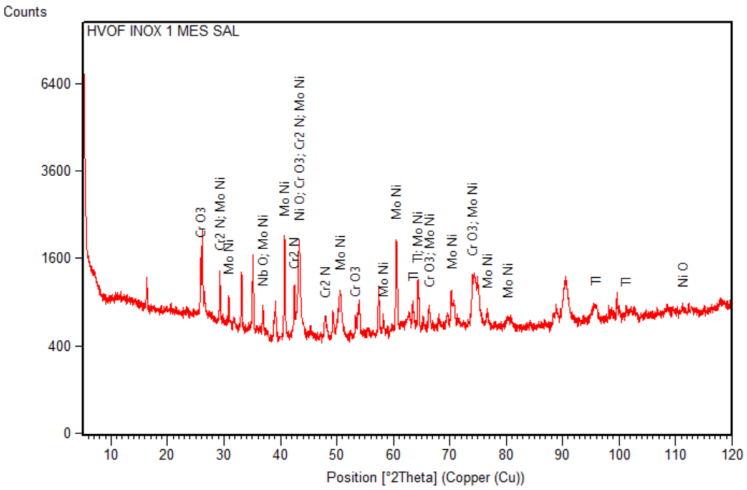

17 c)

Figure 17. HVOF INOX diffractograms

First and most importantly, in the first diffractogram the title is putted wrong, because it should be written HVOF INOX NO SALT. By observing HVOF diffractograms, it can be extracted that there are more small peaks than in the CGS spray, which refers to the oxids compounds formed. Once obtained the part side DRX, the situation changes considerably, by the great formation of chromium and nickel oxides and the presence of molybdenum and chromium nitrides. It is noted that the superficial oxidation of the HVOF samples have suffered more oxidation and changeable phases than in the CGS specimens.

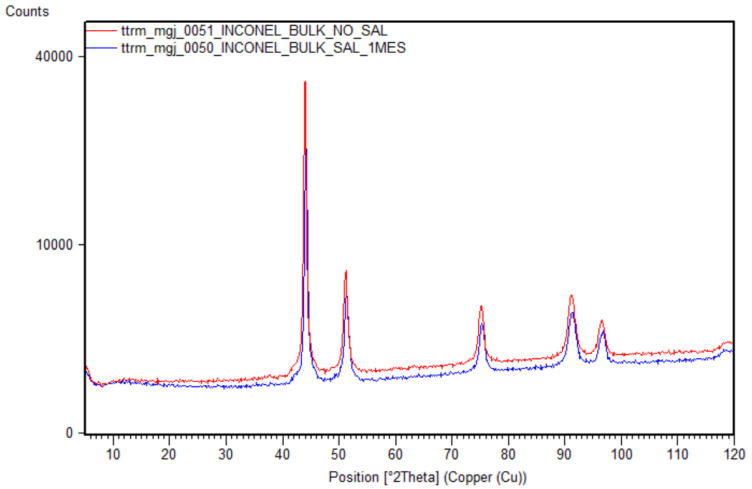

Figure 18. Inconel bulk comparison diffractogram

This final diffractogram shows the results over the Inconel bulk sample. According with the description properties of this alloy, as mentioned before, the Inconel surface has developed high corrosion resistance.

6. CONCLUSIONS

After extracting the results of the study, the following statements can be concluded.

To begin with, it has been possible to verify the successful preparation of the substrate surface, blasting with alumina, thus causing an efficient adhesion of the Inconel625 coating over the stainless-steel surface.

After working with two of the most widely implemented spraying techniques, it has been determined that the HVOF coatings have maintained a better internal structure. At first sight, in the cases of CGS, the reduction of the thickness has been lower, but its irregular microstructure and with many interparticle spaces have generated an interstitial penetration of the corrosive medium. In the HVOF samples, on the other hand, there has been more thickness reduction, but the good laminar arrangement of the splats formed by melting the Inconel particles resulted in only superficial oxidation.

Photographs of the sample's free surface taken with the FESEM microscope showed that if the experiments had been performed over a longer period, the coating made by CGS would have been removed due to the fact that the interface between the substrate and the coating was not sufficiently connected

Furthermore, it has been noted that a more changeable phase in the coating surface of the HVOF sample has been produced, according to DRX results. However, the oxides formation has promoted the appearance of amorphous phases, but at the same time lower porosity results and denser coatings, which brings to the conclusion that the coating made from HVOF has more resistance to corrosion despite its greater decrease in thickness.

Finally, in accordance with the obtained results, it is possible to confirm that the use of Inconel 625 as a steel protection material in TES tanks enhances the overall corrosion resistance.

7. REFERENCES AND NOTES

1. Naciones Unidas. El papel de los combustibles fósiles en un sistema energético sostenible | Naciones Unidas. *Crónica ONU* (2019).
2. IEA. Technology Roadmap Solar Photovoltaic Energy - International Energy Agency (IEA). *Training for Project Management* (2014).
3. NREL. Enerstar | Concentrating Solar Power Projects. *SOLARPACES* (2017).
4. Goswami, D. Y. *Principles of Solar Engineering, Third Edition*. *PhD Proposal* vol. 1 (2015).
5. Kalogirou, S. A. Solar thermal collectors and applications. *Progress in Energy and Combustion Science* vol. 30 231–295 (2004).
6. Angayarkanni, S. A. & Philip, J. Review on thermal properties of nanofluids: Recent developments. *Advances in Colloid and Interface Science* vol. 225 146–176 (2015).
7. Chen, W., Zou, C. & Li, X. An investigation into the thermophysical and optical properties of SiC/ionic liquid nanofluid for direct absorption solar collector. *Solar Energy Materials and Solar Cells* **163**, 157–163 (2017).
8. Ahmed, S. F., Khalid, M., Rashmi, W., Chan, A. & Shahbaz, K. Recent progress in solar thermal energy storage using nanomaterials. *Renewable and Sustainable Energy Reviews* vol. 67 450–460 (2017).
9. Pawłowski, Lech. *The science and engineering of thermal spray coatings*. (Wiley, 2008).
10. Amin, S. & Panchal, H. *A Review on Thermal Spray Coating Processes*. *International Journal of Current Trends in Engineering & Research* vol. 2 http://www.ijcter.com (2016).

11. HVOF THERMAL SPRAY SYSTEMS. https://www.fst.nl/thermal-spray-equipment/modular-thermal-spray-systems/hvof-spray-systems.html.
12. Akhtari-Zavareh, M. *et al.* Fundamentals and Applications of Thermal Spray Coating Electrochemical modelling of galvanic and localized corrosion processes View project SMART NANOCONCRETES AND CEMENT-BASED MATERIALS: PROPERTIES, MODELLING AND APPLICATIONS View project Fundamentals and Applications of Thermal Spray Coating. *Canadian Journal of Basic and Applied Sciences ©PEARL* **05**, 1–11 (2017).
13. Knight, R. *The HVOF process-The hottest topic in the thermal spray industry*. *Article in Welding Journal* https://www.researchgate.net/publication/234452335 (1993).
14. Li, C. J. *Thermal Spray Process Films and Coatings: Technology and Recent Development Thermal spraying of light alloys Hardmetals*. (2014).
15. Guilemany, J. M., Cinca, N., Dosta, S. & Cano, I. G. FeAl and NbAl 3 intermetallic-HVOF coatings: Structure and properties. *Journal of Thermal Spray Technology* vol. 18 536–545 (2009).
16. Oksa, M., Turunen, E., Suhonen, T., Varis, T. & Hannula, S. P. Optimization and characterization of high velocity oxy-fuel sprayed coatings: Techniques, materials, and applications. *Coatings* **1**, 17–52 (2011).
17. Pontarollo, A., Progetti, E. & Guidolin, M. *Characterisation of Inconel 625 coatings deposited by cold spray Die Casting View project FCW products and processes View project*. https://www.researchgate.net/publication/289522915 (2011).
18. Fantozzi, D., Matikainen, V., Uusitalo, M., Koivuluoto, H. & Vuoristo, P. Chlorine-induced high temperature corrosion of Inconel 625 sprayed coatings deposited with different thermal spray techniques. *Surface and Coatings Technology* **318**, 233–243 (2017).
19. Guilemany, J. M. & Dosta, S. *Cold Gas Spray: Innovative Technology in Surface Engineering-New Bulk Metallic Glasses*

and Composites View project THERMAL SPRAY COATINGS/COLD GAS SPRAY AND ADDITIVE MANUFACTURE View project. https://www.researchgate.net/publication/326225480 (2014).

20. Cavaliere, P. *et al.* Microstructural and fatigue behavior of cold sprayed Ni-based superalloys coatings. *Surface and Coatings Technology* **324**, 390–402 (2017).
21. Shankar, V., Bhanu, K., Rao, S. & Mannan, S. L. *Letter to the Editors Microstructure and mechanical properties of Inconel 625 superalloy*. www.elsevier.nl/locate/jnucmat.
22. *Fritsch GmbH • Milling and Sizing Laser Scattering-A brief Introduction*. www.fritsch.de.
23. Standard Guide for Metallographic Preparation of Thermal Sprayed Coatings 1. doi:10.1520/E1920-03R14.
24. Sergi, A., Khan, R. H. U. & Attallah, M. M. The role of powder atomisation route on the microstructure and mechanical properties of hot isostatically pressed Inconel 625. *Materials Science and Engineering A* **808**, (2021).
25. de CONTAMINACIÓN B Chico, M. Y., de la Fuente, D. & Simancas Morcillo, J. M. *CORROSIÓN ATMOSFÉRICA DE METALES. EFECTO DE PARÁMETROS*.
26. Mohammadi Zahrani, E. & Alfantazi, A. M. Hot corrosion of Inconel 625 wrought alloy and weld overlay on carbon steel by gas metal arc welding in 47 PbSO4-23 ZnO-13 Pb3O4-7 PbCl2-5 CdO-5 Fe2O3 molten salt mixture. *Corrosion Science* **183**, (2021).
27. Goods, S. H. & Bradshaw, R. W. Corrosion of Stainless Steels and Carbon Steel by Molten Mixtures of Commercial Nitrate Salts. *Journal of Materials Engineering and Performance* **13**, (2004).
28. Goods, S., Bradshaw, R., Prairie, M. & Chavez, J. *Corrosion of stainless and carbon steels in molten mixtures of industrial nitrates*. (1994) doi:10.2172/10141843.
29. Sandoval-Amador, A., Jaimes-Campos, A. G., Mogollón-Sanabria, A. X., Estupiñán-Duran, H. A. & Peña-Ballesteros, D. Y. Corrosión a alta temperatura del acero inoxidable AISI

316L en termofluidos a base de sales de nitrato fundido para plantas de concentración solar. *Matéria (Rio de Janeiro)* **25**, (2020).

30. Portella, M. O. G. *et al.* Atmospheric corrosion rates of copper, galvanized steel, carbon steel and aluminum in the metropolitan region of Salvador, BA, Northeast Brazil. in *Procedia Engineering* vol. 42 171–185 (Elsevier Ltd, 2012).
31. Sandoval-Amador, A., Santander-Vega, A. J., Amaya-Cáceres, C. C., Estupiñán-Duran, H. A. & Peña-Ballesteros, D. Y. 316L stainless steel corrosion in molten salts NaNO3 KNO3 NaNO2 simulating storage conditions. in *Journal of Physics: Conference Series* vol. 1159 (Institute of Physics Publishing, 2019).
32. Fantozzi, D., Matikainen, V., Uusitalo, M., Koivuluoto, H. & Vuoristo, P. Chlorine-induced high temperature corrosion of Inconel 625 sprayed coatings deposited with different thermal spray techniques. *Surface and Coatings Technology* **318**, 233–243 (2017).
33. Griekspoor thermal coatings.

8. ACRONYMS

CSP:	**Concentrated Solar Power**
TES:	**Thermal Energy Storage**
HVOF:	**High Velocity Oxygen-Fuel**
OM:	**Optical microscopy**
SEM:	**Scanning electron microscopy**
FESEM:	**File Emission Scanning Electron Microscopy**
CGS:	**Cold Gas Spray**

APPENDICES

APPENDIX 1: THICKNESS MEASUREMENT TABLES OF ONE WEEK CORROSION TEST

	CGS INOX SAL	CGS INOX no SAL	HVOF INOX SAL	HVOF INOX no SAL
	239,909	222,397	231,136	246,494
	245,379	220,25	238,804	235,52
	249,758	186,226	244,283	249,76
	219,097	226,754	236,613	259,617
	173,092	226,765	228,987	237,708
	221,277	200,467	235,54	236,676
	236,615	240,997	243,195	242,13
	213,612	246,482	251,97	249,78
	225,661	243,195	235,517	270,627
	203,75	248,672	244,283	239,909
	203,753	230,082	257,435	248,701
	211,443	238,806	256,352	239,902
	237,708	170,891	240,997	248,684
	217,993	181,871	245,386	237,711
	175,269	174,177	253,082	226,754
	215,8	182,94	253,047	236,613
	226,765	199,368	246,494	257,447
	246,511	207,036	251,97	251,958
	204,848	243,195	242,112	265,102
	244,32	245,376	248,684	256,333
	210,325	266,192	244,283	242,112
	178,558	245,379	256,331	247,628
	226,754	258,524	249,78	270,591
	230,04	213,612	261,865	233,329
	217,993	212,539	253,066	226,757
	233,337	237,718	255,273	255,235
	244,283	248,665	247,57	262,906
	251,951	244,283	253,047	259,626
	243,188	222,383	247,577	248,665
	215,8	215,8	227,892	233,327
MITJANA	**222,160**	**223,368**	**246,086**	**247,253**
DESV.ESTÀNDARD	**21,294**	**25,903**	**8,777**	**12,014**
RED.ESPESSOR	**1,208**		**1,168**	

	CGS INOX SAL	CGS INOX no SAL	HVOF INOX SAL	HVOF INOX no SAL
	222,375	176,378	267,287	233,350
	215,800	230,043	276,057	239,989
	193,894	232,231	282,528	225,659
	238,806	215,800	268,416	239,902
	227,852	239,902	285,941	236,653
	225,659	204,857	272,762	255,256
	250,863	217,993	294,673	227,860
	233,327	219,111	280,439	239,909
	208,143	225,669	278,248	230,051
	244,281	227,873	272,764	243,208
	193,919	260,722	246,472	247,589
	233,350	214,707	239,902	255,235
	224,587	260,715	236,615	238,804
	196,094	173,078	248,672	254,142
	179,654	167,615	249,758	248,663
	242,093	208,135	240,997	242,093
	225,669	247,570	227,852	247,570
	247,570	215,803	238,814	230,040
	207,036	250,853	247,589	222,397
	209,253	236,623	262,905	225,683
	243,185	245,379	237,731	230,064
	201,571	238,806	238,806	232,241
	211,463	262,903	233,337	248,672
	222,375	242,100	238,806	245,376
	174,177	209,227	258,524	239,922
	241,005	250,863	232,234	258,559
	227,849	245,415	238,955	233,350
	192,799	224,574	234,425	243,188
	240,997	264,008	235,528	242,112
	200,467	245,415	243,185	231,159
MITJANA	**219,204**	**228,479**	**253,674**	**239,623**
DESV.ESTÀNDARD	**20,973**	**25,475**	**19,361**	**9,707**
RED.ESPESSOR	**9,275**		**14,051**	